Phase transition of vortexlike self-propelled particles induced by a hostile particle

Haibin Duan* and Xiangyin Zhang
Bio-inspired Autonomous Flight Systems (BAFS) Research Group, School of Automation Science and Electrical Engineering, Beihang University, Beijing 100191, People's Republic of China
(Received 25 January 2015; published 1 July 2015)

When encountering a hostile particle, the avoidance behaviors of the vortex state of self-propelled particles exhibit phase transition phenomena such that the vortex state can change into a crystal state. Based on the self-propelled particle model and a molecular dynamics simulation, the dynamic response of the vortex swarm induced by a hostile particle (predator or obstacle) is studied. Three parameters are defined to characterize the collective escaping behaviors, including the order parameter, the flock size, and the roundness parameter. If a predator moves slower with a larger risk radius, the vortex swarm cannot return to its original vortex state, but rather transforms into a crystal state. The critical phase transition radius, the maximum risk radius of a predator with which the transition from a vortex to crystal state cannot take place, is also examined by considering the influence of the model parameters. To some degree, the critical radius reflects the stability and robustness of the vortex swarm.

DOI: 10.1103/PhysRevE.92.012701 PACS number(s): 87.10.−e, 05.45.Xt, 05.65.+b, 89.75.Fb

I. INTRODUCTION

The collective motion of large aggregations of animals is one of the most fascinating phenomena in the living world [1], which often exists in mammals, fish, insects, and birds for various benefits, such as an easier search for food, higher mating efficiency, and more successful predator avoidance [2]. Prominent examples of collective motion are bird flocks, fish schools, and mammal herds. Interaction via an intermediate field is one of the major mechanisms in those organisms [3,4]. Vicsek *et al.* indicated that collective behavior is a key concept in highly multidisciplinary fields, including ethology, evolutionary biology, control theory, economics, and social sciences [5]. Most existing studies have modeled collective motion through simulation via two frameworks: Eulerian models and Lagrangian models [6]. The Eulerian models frequently use the flock density as a key variable to present the space-time dynamics of a flock. The Lagrangian models consider the individual animals as pointlike particles, which are also called self-propelled particles (SPPs), and apply some social interaction rules to them [7].

Generally, the SPP system can exhibit distinct stable phases, such as an order crystal and a vortex. In the crystal phase, all particles move in the same direction and are equally spaced within a disk-shaped region [8]; while in the vortex phase, all particles rotate around a common center and form a ring shape. In nature, vortexlike behavior can be observed in a wide range of biological systems, such as a rotating colony of army ants, sperm cells, bacterial colonies, and fish milling. Recently, an increasing number of researchers have focused on a steady vortex flock, including both theorists and experimentalists [9,10]. Levine *et al.* [11] investigated both discrete and continuum models consisting of SPPs that obey simple interaction rules, and show that the vortex solution can be obtained from random initial conditions, even in the absence of a confining boundary. Erdmann *et al.* [12] found that, for strong noise, the translational motion of a swarm of SPPs suddenly becomes impossible and is abruptly replaced by a vortex flock. Chen *et al.* [13] presented particle-based simulations and a continuum theory for steady rotating flocks formed by SPPs in two-dimensional space, and found steady rotating flocks when the velocity of the particles lacked long-range alignment. You *et al.* [14] studied the collective behaviors of two-component swarms in a vortex state, and showed that a mass difference can introduce a protective behavior for the lighter members of the swarm.

In this article, we focus on the phase stability and transitions of vortex SPPs. The vortexlike behavior of SPPs usually cannot be easily destroyed [9]. Existing research [8] has investigated the stability of the vortex phase when subjected to a uniform impulse hitting force, and according to their findings, when an abrupt hitting force is larger than the critical value, the vortex flock will cross over to the crystal phase and never return. Other than external impulse perturbations, it is more common that the collective motion state is destroyed by hostile individuals, which can be predators or obstacles that should be kept away from. Different from impulse perturbations, when the swarm encounters predators or obstacles, lasting external perturbations will affect the swarm, and, meanwhile, only parts rather than all of the particles will be affected by external perturbations at the same time. Lee *et al.* [15,16] finds that crystal flocks can return to the original crystal state form after a predator's attack has broken the formation. However, the behaviors of SPPs in the vortex phase when hostile particles exist, such as predators, still need to be reported. By utilizing a molecular dynamics (MD) simulation, the main interest of this article is to examine the dynamic response of a vortexlike SPP system, and study how strongly the vortex phase of SPPs is maintained when encountering perturbation from a hostile particle.

II. MODEL DESCRIPTION

A particle-based model is used to represent the motions of SPPs, which obey Newtonian dynamics [9–17]. Consider a swarm system consisting of N particles, in which the motion

*Author to whom correspondence should be addressed: hbduan@buaa.edu.cn

of each particle is governed by the following equation,

$$m_i \frac{d\vec{v}_i}{dt} = \vec{f}_i^{\text{align}} + \vec{f}_i^{\text{body}} + \vec{f}_i^{\text{fric}} + \vec{f}_i^{\text{avoid}}, \quad \frac{d\vec{x}_i}{dt} = \vec{v}_i, \quad (1)$$

where m_i, $\vec{x}_i$, and $\vec{v}_i$ are the mass, position, and velocity vector of the individual ith particle, respectively. The four terms $\vec{f}_i$ represent various types of forces acting upon the ith particle, including the aligning force $\vec{f}_i^{\text{align}}$, the body force $\vec{f}_i^{\text{body}}$, the friction force $\vec{f}_i^{\text{fric}}$, and the avoiding force $\vec{f}_i^{\text{avoid}}$.

The first force term accounts for the self-propelling force [14] and makes each particle align its velocity with its neighboring particles,

$$\vec{f}_i^{\text{align}} = a\hat{V}_i, \quad (2)$$

where a represents the propelling strength and $\hat{V}_i = \vec{V}_i/|\vec{V}_i|$ is the unit vector parallel to $\vec{V}_i$, which is defined as

$$\vec{V}_i = \sum_{j=1}^{N} \exp(-R_{ji}/r_a)\vec{v}_j, \quad (3)$$

where $R_{ji} = |\vec{x}_i - \vec{x}_j|$ is the distance between the ith and jth particles, and r_a is the parameter controlling the range of alignment. A larger value of r_a can enhance the tendency for synchronized motion [14]. Note that, although there is no explicit individual propulsion force in the motion equation (1), actually, a constant propulsion component is implicit in the above alignment interaction. The sum in Eq. (3) contains the velocity item $\vec{v}_i$ of the focal particle itself, and thus it can serve as an energy pump to propel the active motion of the particles.

The second force term describes the mutual interaction forces between particles. Particles attract each other to get close, and, meanwhile, they avoid colliding into each other. A Lennard-Jones potential type of expression is adopted to model the body force as follows,

$$\vec{f}_i^{\text{body}} = b\sum_{j\neq i}^{N} (1 - R_{ji}/r_b)\exp(-R_{ji}/r_b)\hat{R}_{ji}, \quad (4)$$

where $\hat{R}_{ji} = (\vec{x}_i - \vec{x}_j)/|\vec{x}_i - \vec{x}_j|$ is the unit vector directed to the ith particle from the jth particle. b and r_b denote the force strength and the range between interacting particles, respectively.

The third force term is introduced to prevent particles from moving too fast, which is set to be proportional to the velocity of the ith particle with the friction coefficient γ,

$$\vec{f}_i^{\text{fric}} = -\gamma\vec{v}_i. \quad (5)$$

Particles in the swarm should keep away from hostile predators or threatening obstacles. The movement of the predator is expressed as

$$\vec{v}_p = \kappa \cdot \hat{v}_p, \quad \frac{d\vec{x}_p}{dt} = \vec{v}_p, \quad (6)$$

where κ denotes the speed of the predator, $\hat{v}_p$ is the direction of motion, and $\vec{x}_p$ and $\vec{v}_p$ represent the position and the velocity vectors of the predator. When particles are in the risk region of a predator, an avoiding force can make the particles move away from the predator. The last force term in Eq. (1) describes the avoidance behaviors of particles to predators, which is defined as follows [15],

$$\vec{f}_i^{\text{avoid}} = \frac{c}{1 + \exp[\omega(R_{pi} - R)]}\hat{R}_{pi}, \quad (7)$$

where c and ω are two constants that characterize the strength of the avoiding force. R is the radius of the predation risk. $R_{pi} = |\vec{x}_i - \vec{x}_p|$ denotes the distance between the predator and the ith particle, and $\hat{R}_{pi} = (\vec{x}_i - \vec{x}_p)/|\vec{x}_i - \vec{x}_p|$ is the unit direction vector.

III. RESULTS AND ANALYSIS

A. Vortex formation

This article only considers the collective behavior in two spatial dimensions. Initially, $N = 100$ particles are randomly distributed with a random velocity, as shown in Fig. 1(a). The movements of all particles obey the behavioral rules given in Eq. (1). Given various values of r_a, the swarm can evolve into different steady states. With a sufficiently large r_a, for example, $r_a = 1$, the system finally forms a stationary crystal, as shown in Fig. 1(b). With a small enough r_a, for example, $r_a = 0.05$, particles evolve into a stationary vortex in which

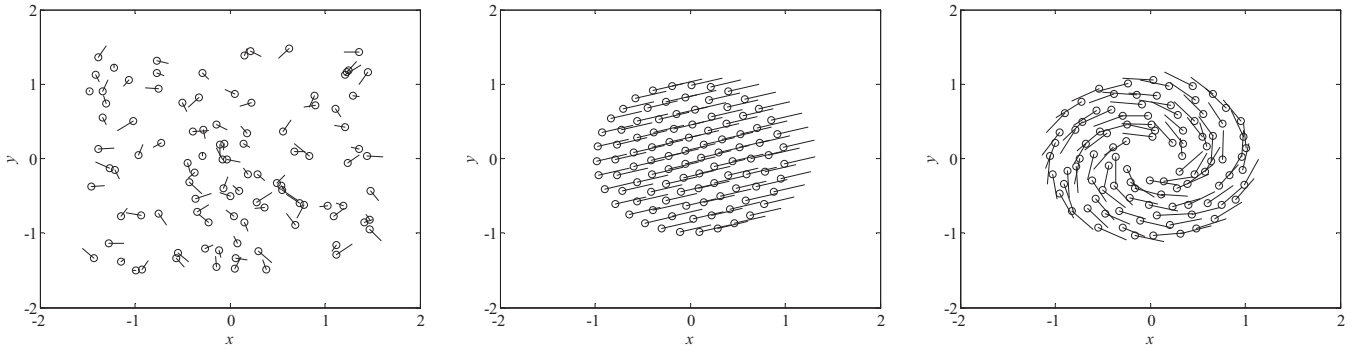

FIG. 1. Snapshots showing the typical steady states of the swarm. The black solid dots show the positions of particles in the swarm. Each particle moves in the direction of the line segments from the dot, with the velocity proportional to the length. (a) The randomly initial positions and velocity of 200 individuals. (b) A snapshot of the steady marching crystal with $r_a = 1$. (c) A snapshot of the steady rotating vortex with $r_a = 0.05$. Other parameters are set as $N = 100$, $m = 1$, $\gamma = 1$, $a = 1$, $b = 1$, $r_b = 2$.

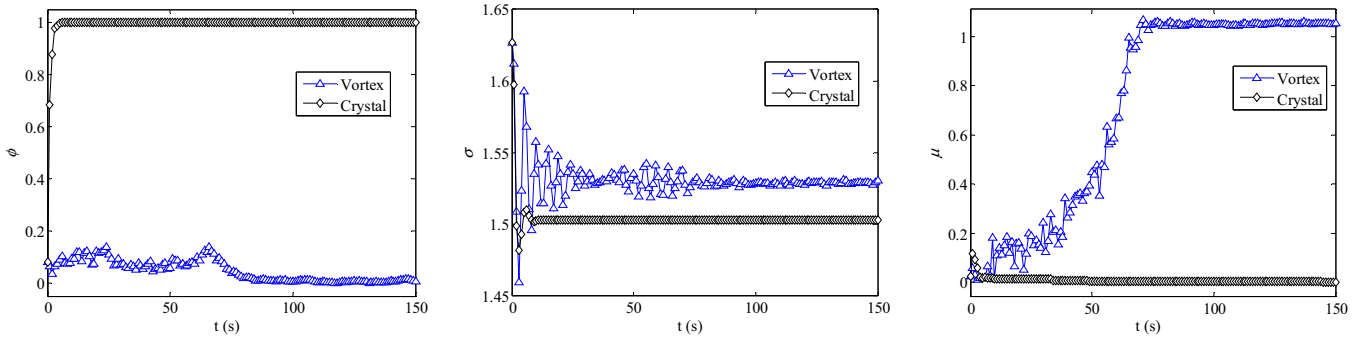

FIG. 2. (Color online) Time evolution of (a) the order parameter ϕ, (b) the flock size σ, and (c) the flock roundness parameter μ when forming the crystal and vortex states.

all individuals rotate around a common center, as shown in Fig. 1(c).

Various parameters are defined to further investigate the collective motion state. The absolute value of the average velocity is used to represent the nature of synchronization in the swarm [5],

$$\phi = \frac{1}{N}\left|\sum_{i}^{N} \hat{v}_i\right|, \tag{8}$$

where N is the number of particles in the swarm, and $\hat{v}_i$ denotes the unit vector that goes along the velocity of the ith particle. ϕ can be considered as the order parameter taking a value in the range [0,1] and shows a tendency for the particles to move in the same direction. If all the particles move in the same direction, the value of ϕ will be close to one, whereas if all the particles move randomly, the value of ϕ will be approximately zero [5]. Figure 2(a) shows the time evolution of the order parameter for a swarm with various r_a. Both the simulation curves start from the disordered state, as shown in Fig. 1(a), with $\phi(t=0) \approx 0$. When $r_a = 1$, the order parameter rapidly reaches $\phi = 1$ [black line in Fig. 2(a)], and the swarm achieves a crystal configuration, in which all individuals show an aligned movement [Fig. 1(b)]. When $r_a = 0.05$, the order parameter moves closer to zero [blue line in Fig. 2(a)] than the initial disordered state when the particles eventually show a rotating vortex movement [Fig. 1(c)].

The following parameter is defined to check the size of the flock [15,16],

$$\sigma = \sqrt{\frac{1}{N}\sum_{i}^{N} {r_i}^2}, \tag{9}$$

where $r_i = |\vec{x}_i - \vec{x}_c|$ is the distance from the swarm center $\vec{x}_c$ to the ith particle. The time evolution of the flock size in the process of forming crystal and vortex states is shown in Fig. 2(b), which indicates that the flock size of the vortex swarm is larger than that of the crystal swarm.

Finally, we introduce the roundness parameter to assess the rotating vortex state being defined as

$$\mu = \frac{2}{\pi N}\sum_{i}^{N} \theta_i, \tag{10}$$

where, for each ith particle, θ_i is the angle between its velocity $\vec{v}_i$ and the radial vector that points from the swarm center to the its position $\vec{x}_i$. For a steady vortex flock where all particles rotate in the same direction and the whole swarm forms a perfect round shape, the value of μ is close to one, while it is approximately zero when all particles completely move disorderedly or achieve aligned movement. Figure 2(c) shows the time evolution of the roundness parameter when particles gradually form crystal [Fig. 1(b)] and vortex [Fig. 1(c)] states from the disordered state [Fig. 1(a)].

B. Phase transition induced by a hostile particle

In the following sections, we investigate the response of a vortex swarm when avoiding a hostile particle (predator). In some realistic scenarios, the predator usually moves towards the center of the vortex swarm, for example, when a bird attacks a swarm of crabs and when a whale catches a fish school. This type of predation can help to improve the hunting success rate in nature. Here, the predator is originally located outside of the vortex swarm, as shown in Fig. 3, and is designed to move

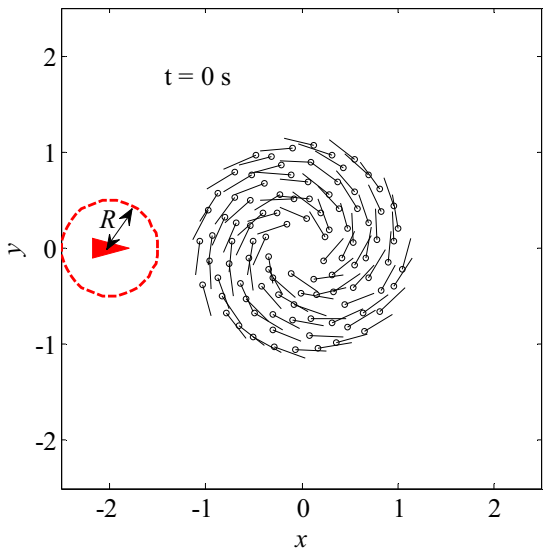

FIG. 3. (Color online) Initial positions of the vortex swarm and a hostile particle. The red arrow shows the direction and position of the hostile particle, and the red circle represents its risk range.

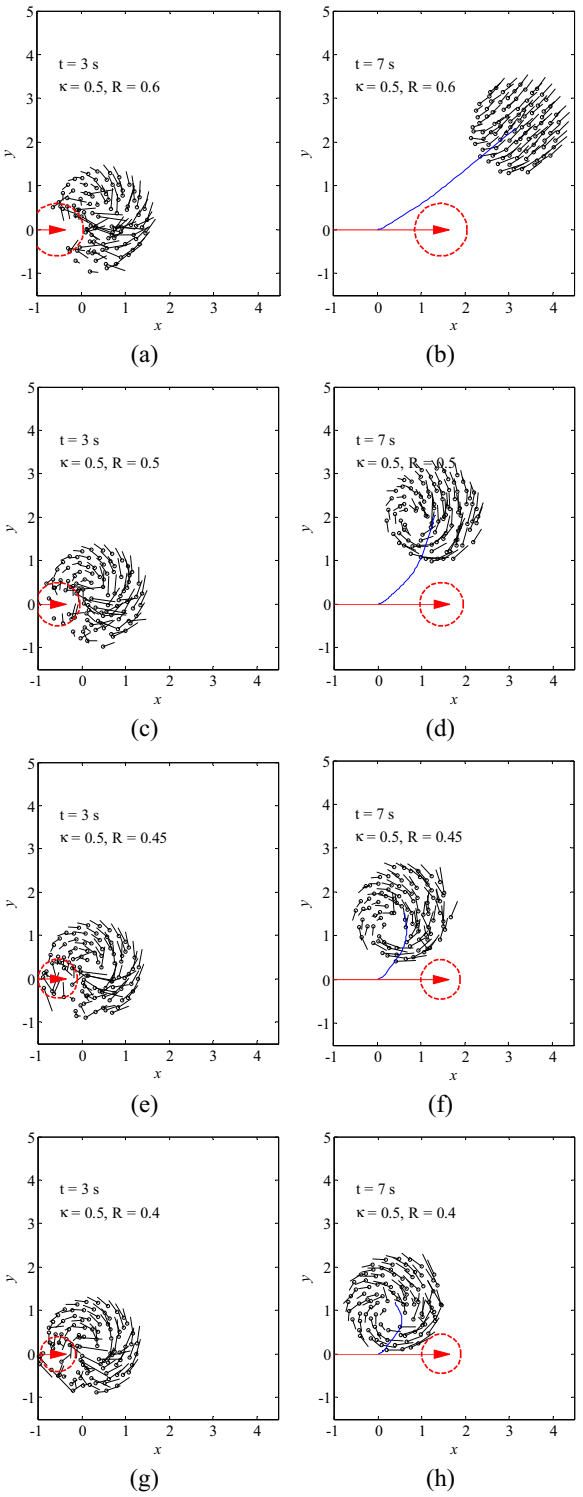

FIG. 4. (Color online) Snapshots showing the response of the vortex swarm when avoiding a predator with a velocity $\kappa = 0.5\ \mathrm{s}^{-1}$. The red circle surrounding the predator (red arrow) shows the radius of the predation risk. For each risk radius ($R = 0.6, 0.5, 0.45, 0.4$) the movements of the swarm at two moments ($t = 3$ and 7 s) are exhibited. The blue line represents the trajectory of the average swarm position. Other parameters are set as $N = 100, m = 1, \gamma = 1, a = 1, b = 1, r_b = 2, c = 10, w = 0.2$.

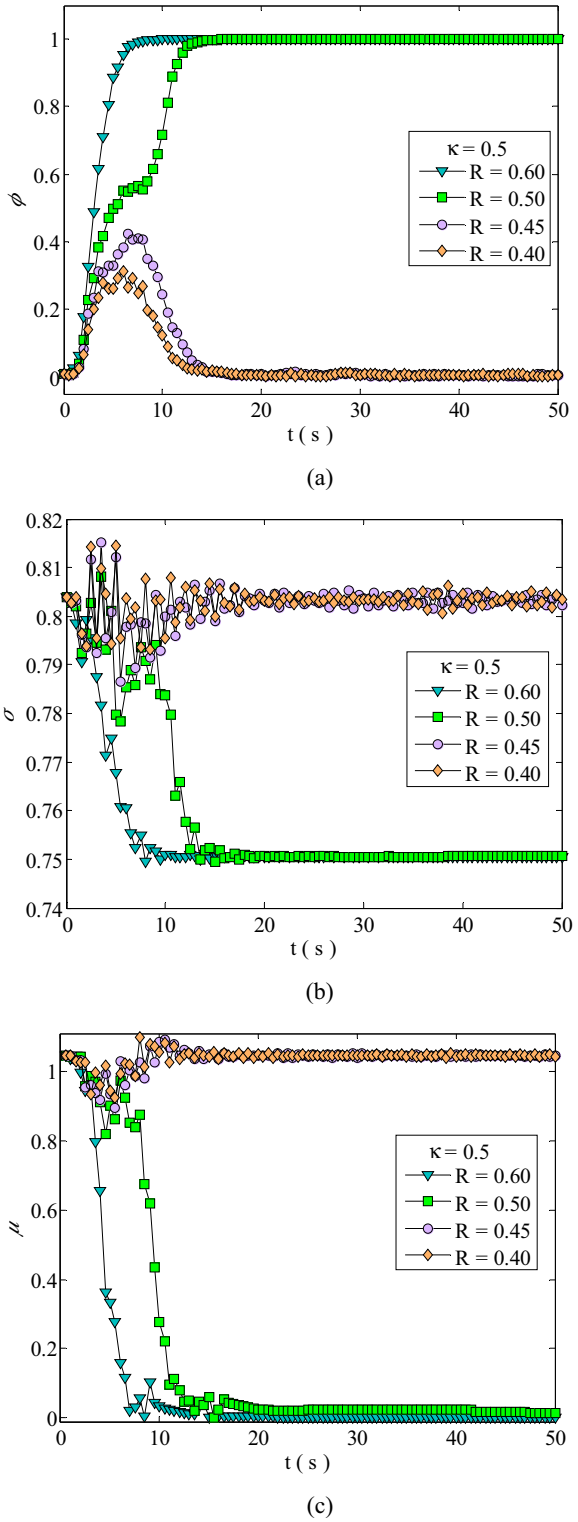

FIG. 5. (Color online) Time evolution of (a) the order parameter ϕ, (b) the flock size σ, and (c) the roundness parameter μ with $\kappa = 0.5\ \mathrm{s}^{-1}$ and various R.

towards the swarm center with a constant speed until it goes through the whole swarm. Since the predator moves straight at the center of the vortex swarm, the initial angular momentum of the predator relative to the whole swarm is approximately zero. The motivation of this article is to investigate the stability of the vortex flock with respect to the hostile particle, and thus we assume that the hostile particle simply rushes into the

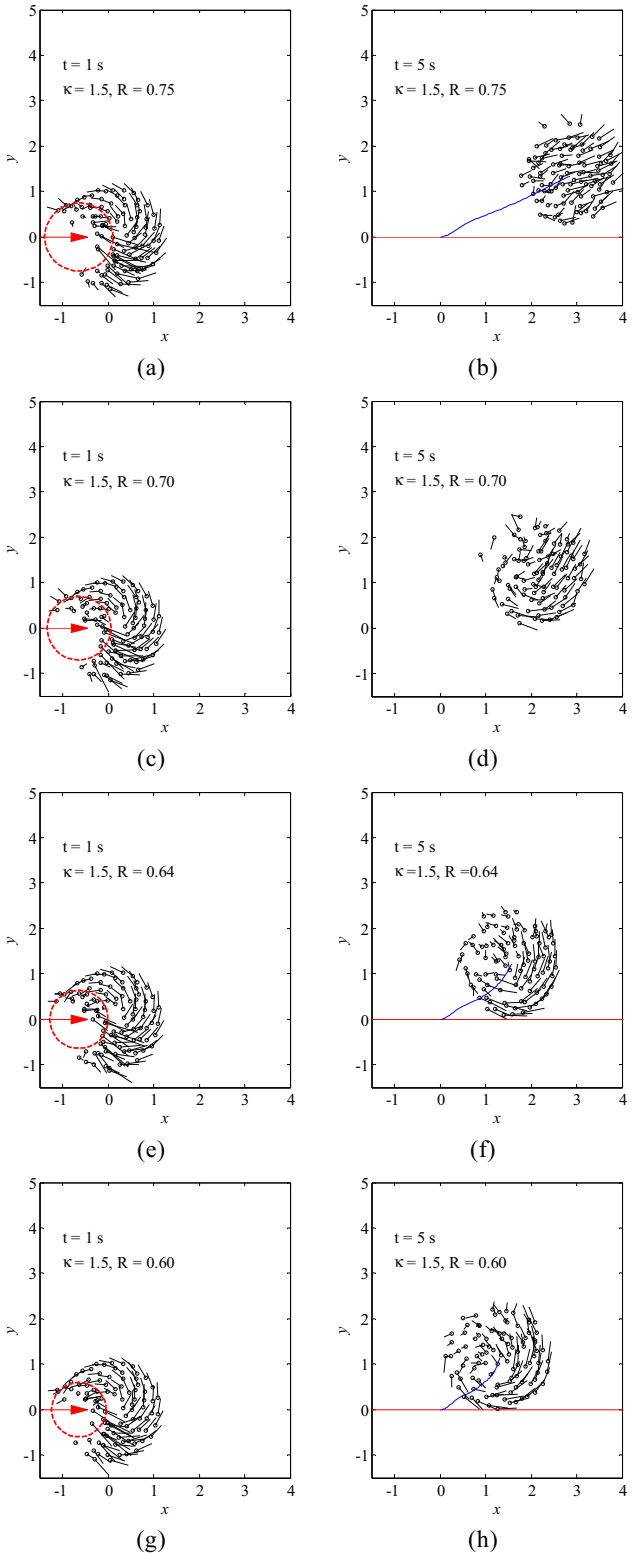

FIG. 6. (Color online) Snapshots showing the response of the vortex swarm under a predator's attack with a velocity $\kappa = 1.5\ \mathrm{s}^{-1}$. The red circle surrounding the predator (red arrow) shows the radius of the predation risk. For each risk radius ($R = 0.75, 0.7, 0.64, 0.6$) movements of the vortex swarm at two moments ($t = 1$ and 5 s) are exhibited. The blue line represents the trajectory of the average swarm position. Other parameters are set as $N = 100, m = 1, \gamma = 1, a = 1, b = 1, r_b = 2, c = 10, w = 0.2$.

vortex flock and moves in a straight line without any response to the changes in the swarm. It is necessary to state that this assumption is more of a physics setting.

For a crystal flock in which all particles align their direction of movement, Lee *et al.* [15,16] observed that a hostile particle's attack can destroy the translational motion state and cause order breaking in the alignment of the swarm. According to their simulation results, the particles that have escaped from the attack intend to reorder the original formulation, and thus the flock finally maintains alignment again [16]. However, if the particles are in a vortex state, the avoiding behaviors in response to the predator or obstacle may induce a change in their collective motion state. The phase transition of the vortex swarm depends on the velocity κ and risk radius R of the predator. By changing the two parameters, we can systematically vary the strength and duration of the perturbation from a nearly vanishing but long time perturbation to a global but short time perturbation. Figures 4(a)–4(h) show various patterns in the vortex swarm with different values of the risk radius $R(R = 0.6,0.5,0.45,0.4$ per unit length), when the attacking velocity is $\kappa = 0.5\ \mathrm{s}^{-1}$. Typical snapshots at 3 and 7 s are presented. When a predator approaches the vortex swarm, the particles in the risk radius of the predator are driven to move away. The initial vortex motion state is disrupted, in that some individuals no longer rotate around the swarm center. As the risk radius increases, more and more particles escape from their original track. The degree of deformation increases with an increase in the risk radius R. If the risk radius is small, those dispersed particles can gradually reform the vortex swarm, as shown in Figs. 4(e)–4(h). However, if the risk radius is large, particles tend to align their movements and eventually transform into the crystal phase, as is shown in Figs. 4(a)–4(d).

Temporal changes in the order parameter, the flock size, and the roundness parameter can be observed in Figs. 5(a)–5(c). Similar to the crystal flock [15], the temporal patterns of the vortex swarm can be roughly divided into different regimes. Initially, all particles rotate about a common center and the interaction body forces among particles provide a centripetal force. When a predator attacks the vortex swarm, particles are forced to move away from their original motion track, and thus the balance of movement is broken. As the predator moves on, the particles that escape from the predator's risk radius begin to reorder their movements. During the escape, the particles can align their movements, and lead those other particles to follow them without being attacked. When the risk radius R is smaller, fewer particles exhibit escaping behavior and the destruction degree of the swarm is also lower, and thus the particles can reform their original rotating motion. However, when R is larger, more particles escape from the predator and the tendency for the whole swarm to align competes with rotation. Eventually, the vortex swarm transforms into the crystal state.

We further check the response of the vortex swarm when the predator attacks at a higher velocity. Figures 6(a)–6(h) show how the particles respond to avoid the predator with a velocity $\kappa = 1.5\,\mathrm{s}^{-1}$ and various risk radii ($R = 0.75, 0.7, 0.64, 0.6$ per unit length), where typical snapshots of the swarm system at two moments ($t = 1$ and 5 s) can be observed. The corresponding time evolution of the order parameter, the flock size, and the roundness parameter with

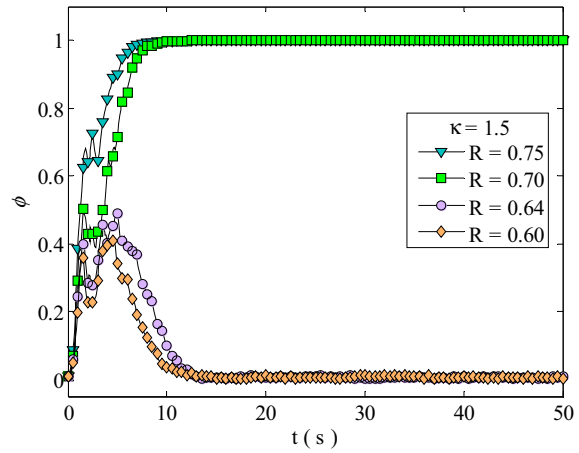

(a)

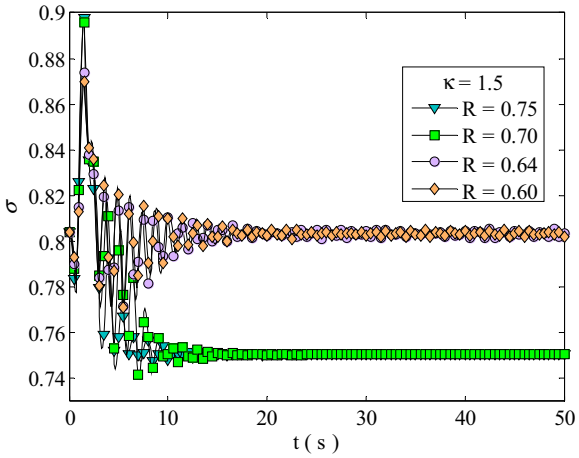

(b)

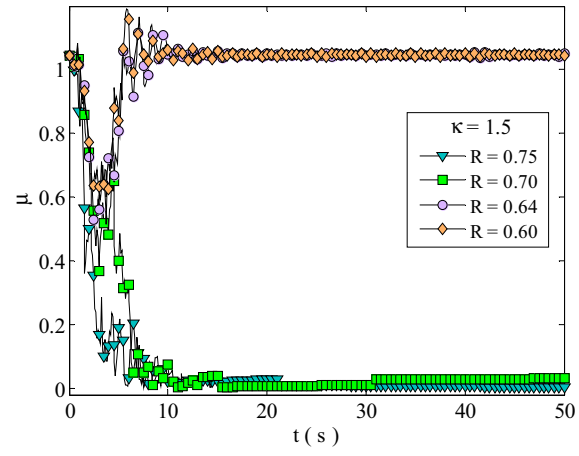

(c)

FIG. 7. (Color online) Time evolution of (a) the order parameter ϕ, (b) the flock size σ, and (c) the roundness parameter μ with $\kappa = 1.5\ \mathrm{s}^{-1}$ and various R.

various risk radii is shown in Fig. 7. Compared with the response of the vortex swarm shown in Fig. 4, particles show a relatively soft reaction, and the formation does not greatly change. In addition, comparing Figs. 6(g) and 6(h) with Figs. 4(a) and 4(b) where the predator has the same risk range

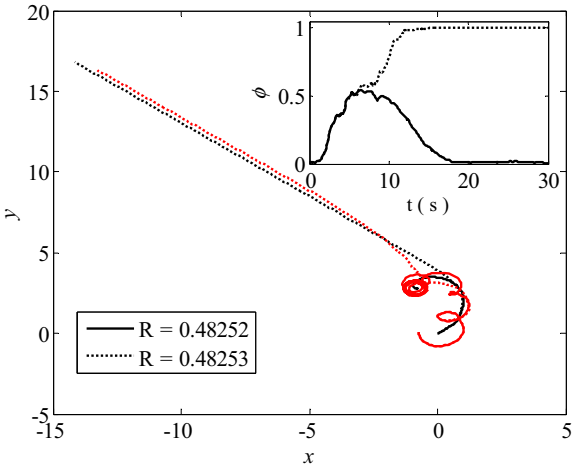

FIG. 8. (Color online) Trajectories of the average swarm position (black lines) and of a single particle (red lines) are shown with different predator risk radii $R = 0.482\,52$ (dotted lines) and $R = 0.482\,53$ (solid lines). The inlay shows the corresponding time evolution of the order parameter. Other parameters are set as $N = 100$, $m = 1$, $\gamma = 1$, $a = 1$, $b = 1$, $r_\mathrm{b} = 2$, $c = 10$, $w = 0.2$, and $\kappa = 0.5\ \mathrm{s}^{-1}$.

$R = 0.6$, it can be observed that, when the predator moves quickly, the particles do not have enough time to escape and can be more likely to reorder into the original vortex state.

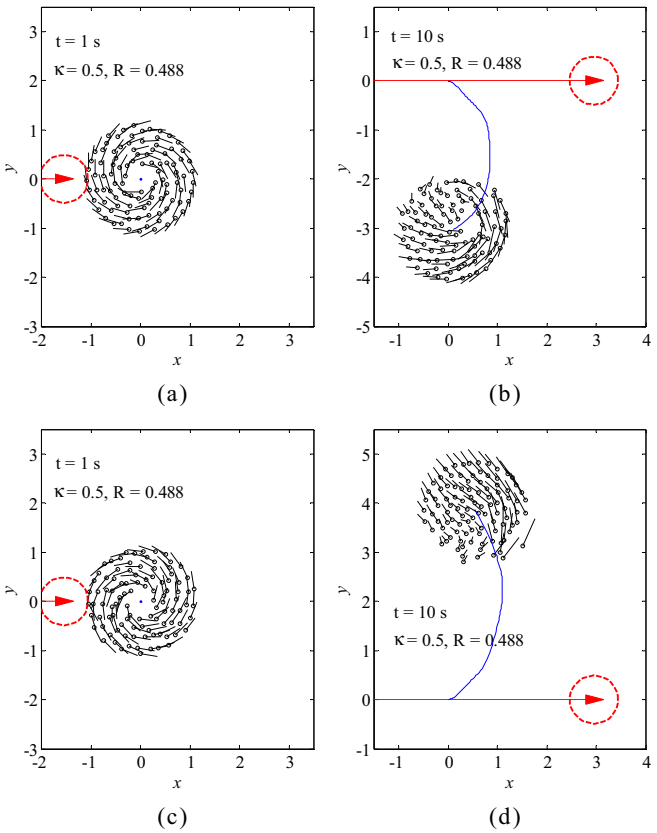

FIG. 9. (Color online) Snapshots showing the transition and no transition phenomena of the vortex swarm under a predator's attack when SPPs inside the vortex flock rotate in both the clockwise and counterclockwise directions.

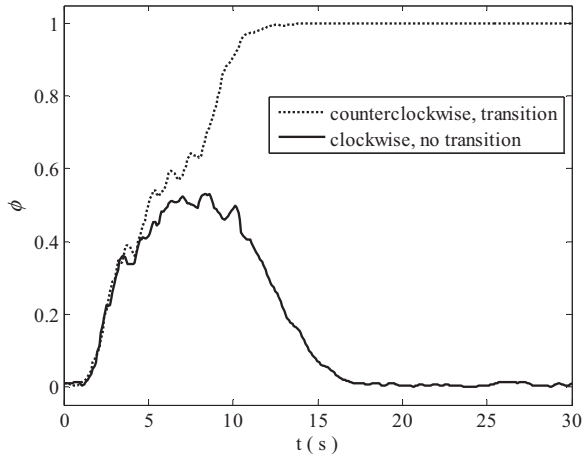

FIG. 10. Time evolution of the order parameter ϕ when the transition takes place from the counterclockwise vortex motion and the transition does not take place from the clockwise vortex motion.

However, a large enough risk range can also force particles to change their motion state and transform into a crystal flock [Figs. 6(a)–6(d)].

Above all, it can be concluded that the phase change in the vortex swarm induced by avoidance behaviors to the predator depends on both the velocity and risk radius of the predator. For a vortex swarm system, the transition into a crystal phase movement appears when the predator moves slower with a larger risk radius. As the velocity κ increases, the transition tendency decreases, because the particles do not have sufficient time to respond to the hostile particle's attack. The tendency for escaped particles to reform into the crystal state increases as the risk radius of the predator increases. There exists a critical radius $R_{\rm cr}$ for each velocity, and the critical radius increases with the predator's velocity. To some degree, the critical radius can reflect the capacity of resisting disturbance and the stability of the vortex swarm. It can be observed that the critical radius increases as the velocity increases. The vortex swarm has more tendencies to return to the original vortex phase, if the predator moves with a faster velocity and a smaller risk radius.

We compare the trajectories of the swarm center and of the same single particle in two scenarios in which the transition does and does not take place, as is shown in Fig. 8. Here, we choose two close values of the risk radius of the predator, $R = 0.482\,52$ and $0.482\,53$. The corresponding trajectories under the two risk radius settings almost overlap before the obvious separation. The transition from the vortex to crystal state induced by the hostile particle's attack is likely to be irreversible unless another distinct perturbation is introduced to the new crystal flock. The comparison curves in the inlay of Fig. 9 indicate that there is a threshold at around $\phi = 0.5$, which has to be crossed for the transition to take place. When the vortex flock encounters an attack from a hostile particle, the escaping behaviors increase the order parameter of the flock. The larger the risk radius of the predator, the faster the order parameter increases. During the limited time that the predator has to impact the flock, once the order parameter of the flock increases to the threshold, the transition from a vortex to crystal state will take place, otherwise the swarm will return to its original vortex state.

The above simulations only consider that the hostile particle moves straight at the initial center of a vortex swarm. However, the center fluctuates when the vortex swam rotates, so a hostile particle cannot accurately aim at the center when rushing into the vortex. Thus, the deviation between the hostile particle's motion direction and the swarm center can produce a nonzero angular momentum of the predator relative to the whole swarm. Next, we consider two special cases when the vortex swarms rotate in a reverse direction. In the two vortex swarms, all SPPs have the same position but opposite velocity. As is shown in Figs. 9(a) and 9(c), the two vortex swarms rotate in the clockwise and counterclockwise directions, respectively. The initial moments of a hostile particle with respect to the vortex center simply have the opposite sign to the angular momentum of the vortex and the others are perfectly identical. When a hostile particle rushes into the swarm with the same risk radius, simulation results show that a counterclockwise rotating swarm can transform into a crystal motion state [Fig. 9(d)], while a clockwise rotating swarm remains at the original vortex state [Fig. 9(b)]. The corresponding time evolution of the order parameter is shown in Fig. 10. It can be explained that, if the moment of the hostile particle with respect to the vortex center has the opposite sign to the angular momentum of the vortex, then the hostile particle will move more against the rotation of the vortex, and thus the motion state of the swarm will more than likely be destroyed. For the simulation results shown in Fig. 9, the vortex that rotates in a

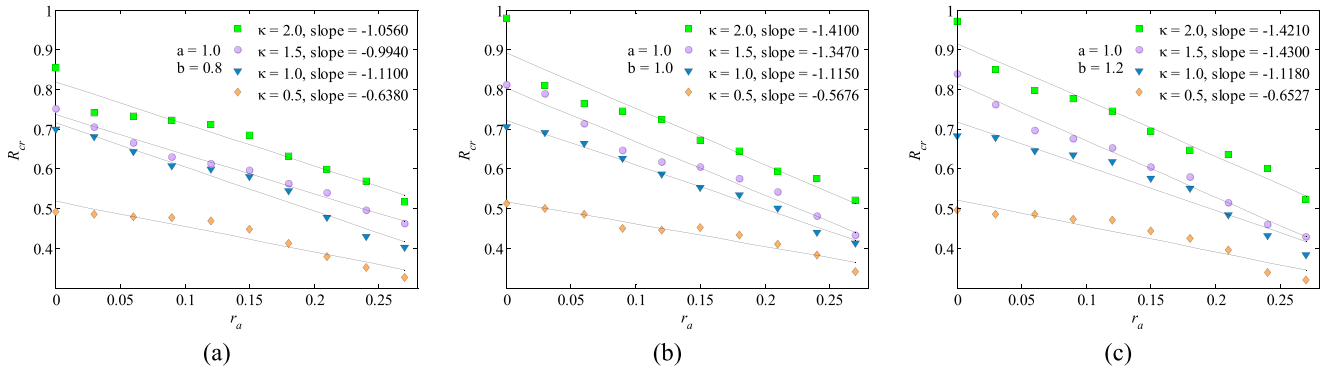

FIG. 11. (Color online) Data of the critical radius $R_{\rm cr}$ vs $r_{\rm a}$ are plotted with respect to various values of b and κ. Solid curves are the linear regression curves of the corresponding data. Other parameters are $N = 100$, $m = 1$, $\gamma = 1$, $a = 1$, $r_{\rm b} = 2$, $c = 10$, $w = 0.2$.

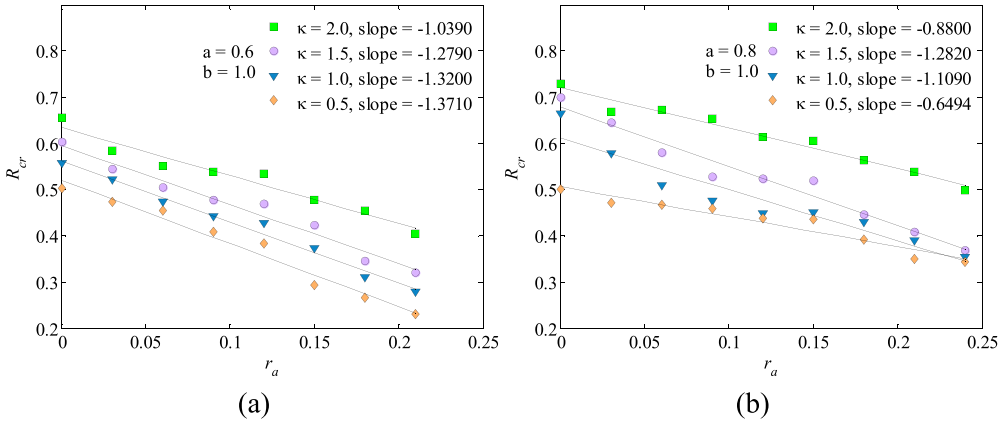

FIG. 12. (Color online) Data of the critical radius R_{cr} vs r_a are plotted with respect to various values of a and κ. Solid curves are the linear regression curves of the corresponding data. Other parameters are $N = 100$, $m = 1$, $\gamma = 1$, $b = 1$, $r_b = 2$, $c = 10$, $w = 0.2$.

clockwise direction has stronger perturbation than that which rotates in a counterclockwise direction.

C. Influence of model parameters

In the following, we examine the vortex swarm's capacity for resisting disturbance by studying the influence of model parameters on the critical radius. Actually, it is hard to determine an accurate critical value of the risk radius, so we define the critical risk radius R_{cr} as the maximum value, with an accuracy of 0.001, under which a vortex to crystal transition does not take place. Figure 11 shows that R_{cr} decreases linearly as the alignment range r_a increases with the same value $a = 1$ and various values of $b = 0.8, 1, 1.2$. The critical radius increases when the predator velocity is large, and, meanwhile, a larger value of b can also result in a more stable vortex swarm and a larger critical phase transition radius. The linear regression curves that describe the linear relationship between R_{cr} and r_a are also plotted.

Figure 12 shows the linearly decreasing relationship between the critical radius R_{cr} and r_a with the parameters $b = 1$ and $a = 0.6, 0.8$. Together with Fig. 11(b), which is obtained with $b = 1$ and $a = 1$, it can be seen that the larger value of a helps to enhance the stability of the vortex swarm, and the vortex phase cannot be easily destroyed and transformed into the crystal state.

The changing process of R_{cr} for a with the parameters $b = 1$ and $r_a = 0.05, 0.1, 0.15$ is shown in Figs. 13 and 14. We can see that R_{cr} is linearly enhanced with increasing propelling strength a. For $\kappa = 1, 1.5, 2.0$, the changing processes between R_{cr} and a fit well the linear relationship, as shown in Fig. 13. However, for $\kappa = 0.5$, thex regression curves are the nonlinear functions $R_{cr} = -Ae^{-Bx} + C$.

IV. CONCLUSIONS

In this article, we have studied the dynamic response of a vortex swarm when avoiding a hostile particle (predator or obstacle) based on the SPP model and the MD simulation. When avoiding a hostile predator, particles in the vortex swarm exhibit different escaping behaviors from those in a crystal swarm. The vortex state shows a phase transition and can transform into a crystal motion state when encountering an attack from a hostile particle. Three parameters are defined to characterize the collective escaping behaviors, including the order parameter, the flock size, and the roundness parameter. The phase transition from a vortex to crystal state when avoiding a single predator depends on both the velocity and risk radius of the predator. When the predator moves slower with a larger risk radius, SPPs in the vortex swarm cannot return to their original vortex state and the transition cannot occur. The critical radius, the maximum risk radius of the predator

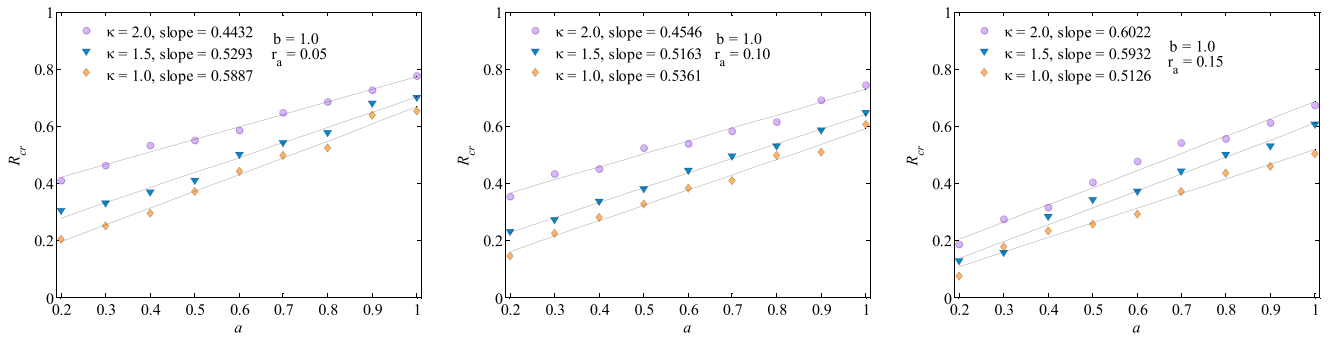

FIG. 13. (Color online) Data of the critical radius R_{cr} vs a are plotted with respect to various values of r_a and κ. Solid curves are the linear regression curves of the corresponding data. Other parameters are $N = 100$, $m = 1$, $\gamma = 1$, $b = 1$, $r_b = 2$, $c = 10$, $w = 0.2$.

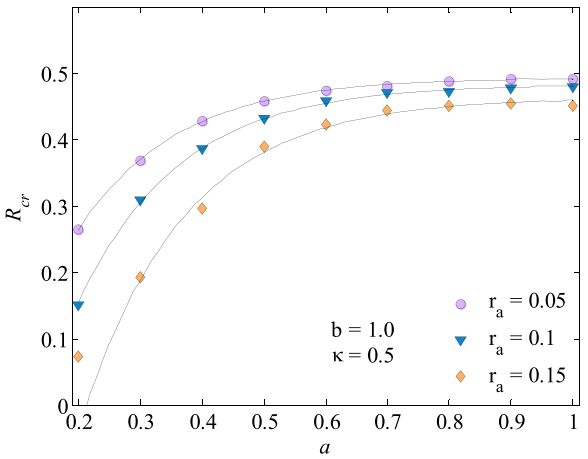

FIG. 14. (Color online) Data of the critical radius $R_{\rm cr}$ vs a are plotted with respect to $\kappa = 0.5$ and various values of $r_{\rm a}$. Solid curves are the fitted functions with the parameters: for $r_{\rm a} = 0.05$, $A = 0.795$, $B = 6.195$, $C = 0.494$; for $r_{\rm a} = 0.10$, $A = 1.176$, $B = 6.347$, $C = 0.482$; and for $r_{\rm a} = 0.15$, $A = 1.682$, $B = 6.026$, $C = 0.464$. Other parameters are $N = 100, m = 1, \gamma = 1, b = 1, r_{\rm b} = 2, c = 10$, $w = 0.2$.

with which the avoiding behavior of the vortex swarm cannot lead to a phase transition, is also examined by considering the influence of model parameters. The conclusion observed is that the critical radius increases as the predator velocity increases. We believe that our study can provide some insight into the dynamic responses of biological swarm systems under external attacks. Our study can be transposed into practical applications, for example, we can drive away a real vortexlike motion swarm (bird flock or fish school) by sending a simple robot (as the hostile particle) to rush into a swarm center. Our future work will focus on the phase transition behavior from the vortex to the crystal from a theoretical point of view [18,19].

ACKNOWLEDGMENTS

This work was partially supported by National Natural Science Foundation of China under Grants No. 61425008, No. 61333004, No. 61273054, and No. 61203223, National Key Basic Research Program of China (973 Project) under Grant No. 2014CB046401, Top-Notch Young Talents Program of China, and the Aeronautical Foundation of China under Grant No. 20135851042.

[1] M. Ballerini, N. Cabibbo, R. Candelier, A. Cavagna, E. Cisbani, I. Giardina, V. Lecomte, A. Orlandi, G. Parisi, A. Procaccini, M. Viale, and V. Zdravkovic, Proc. Natl. Acad. Sci. USA **105**, 1232 (2008).
[2] A. Deutsch, G. Theraulaz, and T. Vicsek, Interface Focus **2**, 689 (2012).
[3] M. Nagy, G. Vásárhelyi, B. Pettita, I. Roberts-Mariania, T. Vicsek, and D. Biroa, Proc. Natl. Acad. Sci. USA **110**, 13049 (2013).
[4] M. Nagy, Z. Ákos, D. Biro, and T. Vicsek, Nature (London) **464**, 890 (2010).
[5] T. Vicsek and A. Zafeiris, Phys. Rep. **517**, 71 (2012).
[6] J. Toner, Y. H. Tu, and S. Ramaswamy, Ann. Phys. (N.Y.) **318**, 170 (2005).
[7] A. Czirók and T. Vicsek, Physica A **281**, 17 (2000).
[8] S. K. You, J. Korean Phys. Soc. **63**, 1134 (2013).
[9] M. H. Mabrouk and C. R. McInnes, Phys. Rev. E **78**, 012903 (2008).
[10] C. R. McInnes, Phys. Rev. E **75**, 032904 (2007).
[11] H. Levine, W. J. Rappel, and I. Cohen, Phys. Rev. E **63**, 017101 (2000).
[12] U. Erdmann, W. Ebeling, and A. S. Mikhailov, Phys. Rev. E **71**, 051904 (2005).
[13] H.-Y. Chen and K.-T. Leung, Phys. Rev. E **73**, 056107 (2006).
[14] S. K. You, D. H. Kwon, Y. I. Park, S. M. Kim, M. H. Chung, and C. K. Kim, J. Theor. Biol. **261**, 494 (2009).
[15] S. H. Lee, Phys. Lett. A **357**, 270 (2006).
[16] S. H. Lee, H. K. Pak, and T. S. Chon, J. Theor. Biol. **240**, 250 (2006).
[17] Y. P. Zhang, H. B. Duan, and X. Y. Zhang, Chin. Phys. Lett. **28**, 040503 (2011).
[18] E. Leeuwen, Å. Brännström, V. A. A. Jansen, U. Dieckmann, and A. G. Rossberg, J. Theor. Biol. **328**, 89 (2013).
[19] J. Strefler, U. Erdmann, and L. Schimansky-Geier, Phys. Rev. E **78**, 031927 (2008).